Deactivation Model Study of High Temperature H$_2$S Wet-Desulfurization by Using ZnO

Arda Hatunoglu [1], **Alessandro Dell'Era** [2,*], **Luca Del Zotto** [3], **Andrea Di Carlo** [4], **Erwin Ciro** [5] **and Enrico Bocci** [1,*]

1   Department of Engineering Sciences, Università degli Studi Guglielmo Marconi, 00193 Rome, Italy; a.hatunoglu@lab.unimarconi.it
2   Department of Basic and Applied Sciences for Engineering, Sapienza University of Rome, 00161 Rome, Italy
3   CREAT, Centro di Ricerca su Energia, Ambiente e Territorio, eCampus University, 22060 Novedrate, Italy; luca.delzotto@uniecampus.it
4   Department of Industrial and Computer Engineering and Economics, University of L'Aquila, 67100 L'Aquila, Italy; andrea.dicarlo1@univaq.it
5   ICMA Department, University Sapienza Rome, Via Eudossiana 18, 00184 Roma, Italy; erwin.ciro@uniroma1.it
*   Correspondence: alessandro.dellera@uniroma1.it (A.D.); e.bocci@unimarconi.it (E.B.)

Abstract: High-temperature desulfurization techniques are fundamental for the development of reliable and efficient conversion systems of low-cost fuels and biomass that answer to the nowadays environmental and energy security issues. This is particularly true for biomass gasification coupled to SOFC systems where the sulfur content has to be minimized before being fed to the SOFC. Thus, commercially available zinc oxide has been studied and characterized as a desulfurizing agent in a fixed-bed reactor at high temperatures from 400 °C to 600 °C. The sorbent material was characterized by XRD, BET, SEM, and EDS analyses before and after adsorption. The sorbent's sorption capacity has been evaluated at different temperatures, as well as the breakthrough curves. Moreover, the kinetic parameters as the initial sorption rate constant k_0, the deactivation rate constant k_d, and the activation energy have been calculated using the linearized deactivation model. The best performances have been obtained at 550 °C, obtaining a sorption capacity of 5.4 g per 100 g of sorbent and a breakthrough time of 2.7 h. These results can be used to extend ZnO desulfurization techniques to a higher temperature than the ones used today (i.e., 550 °C with respect to 400 °C).

Keywords: desulfurization; deactivation model; zinc oxide sorbent; energy

1. Introduction

The conversion of low-cost fuels and biomass is nowadays gaining remarkable relevance as a consequence of the increasing environmental and energy security issues. However, these conversion processes (e.g., gasification) produce organic (tars, sulfur, and nitrogen organic complex substances) and inorganic (sulfur, chlorine, nitrogen, and alkali metals) contaminant compounds that have to be removed to avoid processing plant and environmental issues. Consequently, a significant part of the actual research focuses on developing profitable and efficient gas purification techniques. Among those contaminants, H$_2$S is one of the most problematic. The removal of H$_2$S has been mostly conducted through different kinds of methodologies, such as condensation, catalytic combustion, oxidation reactions, acid gas treatment, and adsorption. Although these methods are recognized for their effectiveness, adsorption is highlighted because of being a prevalent desulfurization treatment, as well as effective in a wide range of working temperatures. Indeed, the low and medium temperature methods (i.e., up to 100 and 250 °C for condensation and adsorption on activated carbon) are mature and efficient techniques but generate waste and suffer from energy inefficiencies requiring one to cool and reheat the gas stream in the recent hot gas applications as gas turbines, high-temperature fuel cells, and hot chemical processes. Metal

oxides, solid mixtures of metal oxides, mixtures of an inert oxide [1–11], zeolites [12–15], activated carbon [16–18], and clays [19,20] are used to carry out the desulfurization process. Among those materials, metal oxides have been deeply studied: Chung et al. [1] studied the H_2S removal by using cobalt-containing sorbent from 300 to 500 °C and obtaining a complete sulfidation after less than 90 min. Otherwise, Ko et al. [2] investigated Zn–Mn-based sorbents supported on silica, zirconia, and alumina at high temperatures (500–700 °C). With a high inlet H_2S concentration of 1×10^4 ppm and a weight hourly space velocity (WHSV) set at 2000 $mLh^{-1}g^{-1}$, the sorbents worked for 15 min before the outlet concentration started to increase considerably. The best working temperature has been reported at 600 °C. Ko et al. [3] analyzed a commercial sorbent based on 30% MnO_x and 60% Fe_2O_3 and 10% inert material. The best working temperature was set at 600 °C with an outgoing flow having less than 10 ppm of H_2S and reaching 120 min before the outlet concentration suddenly became more than 100 ppm. Yasyerli et al. [4] studied the activities of copper oxide and Cu-V and Cu-Mo Mixed Oxides for the H_2S removal between 300 and 700 °C and a flow rate between 100 mL min^{-1} and 160 mL min^{-1}. In this case, the sorbent worked for about 40 min before depleting its desulfurization efficiency. On the other hand, the most notable features related to desulfurization sorbents entail high desulfurization capacity, good chemical stability, fast adsorbing kinetic reactions, and not less important, they are affordable and plentiful [5]. Such characteristics are represented by zinc oxide, largely used in industry [6], being a remarkable H_2S sorbent mainly because of fast kinetic and high stability under reducing conditions. In the available literature, many works refer to the effectiveness of zinc oxide used as a sorbent at temperatures equal to or lower than 400 °C. L. Li et al. studied mesoporous silica materials supported with different ZnO loadings at very low temperatures having a complete sulfidation in an hour or less [7]. Similar work has been performed by Wang et al. [8] by using mesoporous silica with zinc oxide (ZnO) nanoparticles, obtaining comparable results. Kim et al. [9] analyzed a commercially available zinc oxide sorbent with space velocity ranging from 8000 to 24,000 h^{-1} and in a range temperature from 25 to 450 °C. With an inlet H_2S concentration of 2000 ppm, the sorbent has been able to adsorb for 360 min before reaching an outlet concentration of about 3 ppm with 30% of steam into the gas stream sorbent capacity decreases with increasing steam content and increasing space velocity. Furthermore, another process was developed by Rosso et al. [10], which consisted of evaluating ZnO sorbents synthesized by the citrate method. It showed effective H_2S adsorption at 250 °C from 100 to less than 1 ppm, with a breakthrough time of about 9 h, obtained with a space velocity of about 105 h^{-1} and adsorbing up to 31 mg per g of sorbent. Particularly, Jung et al. [11] followed a complete H_2S removal using Zn-based sorbents supported on alumina at 1 atm, 650 °C, and for 400 min. Comparing all these investigations, it is worthwhile to mention that the temperature remained below 650 °C and it is suggested to operate under 450 °C to avoid a critical pathway divided into two steps: (i) zinc oxide or sulfide reduction to elemental zinc, and (ii) sorbent volatilization [21,22]. Recently, energy production by using green technological applications is gaining attention. Such high-tech application comprises the solid oxide fuel cell (SOFC) that enables the electrical energy production from biomass gasification with very high efficiency and low environmental impacts compared to traditional technologies (e.g., biomass gasification coupled to internal combustion engine). This energy production is characterized by an attractive generation of syngas composed of H_2, CH_4, CO, and CO_2, although subsequent purification gas treatments are required to remove hazardous compounds like H_2S. Based on these statements, several works have demonstrated that the optimal H_2S concentration to achieve reliable electrochemical results should be less than 2–3 ppm [23–26]. The processes implementation at higher concentrations can put at risk the proper SOFC operation. Another relevant operative working parameter is the temperature of SOFC (from the 650–750 °C of the anode supported to the 750–850 °C of the other SOFC types) that are similar to the gasification temperature, normally 750–850 °C [23–27]. Thus, it is fundamental to increase the temperature of the intermediate gas conditioning to minimize the energy losses, and in particular for the ZnO sulfur removal process, and

especially for the already commercially available ZnO sorbent that can be applied on large scale. For that reason, in this work, a commercial zinc oxide sorbent for the removal of H_2S, normally used with a temperature ranging from 50–400 °C, has been evaluated in the temperature range between 400 and 600 °C in a fixed-bed reactor, focalizing the attention on not exceeding the safe limit level of H_2S outgoing concentration in more than 2–3 ppm. Also, the sorption capacity has been evaluated and kinetic parameters, as the initial sorption rate constant k_0 and the deactivation rate constant k_d, have been calculated by using the linearized deactivation model. Finally, structural morphological and compositional characterizations have been performed.

2. Experimental Test Bench

The catalytic activity of the selected sorbent was analyzed by feeding N_2, $N_2 + H_2S$, H_2O through the sorbent bed. Corresponding blank tests were considered to understand the behavior of the whole system without any disturbance. The experimental setup of the overall scheme is shown in Figure 1. The detail of each section is explained below.
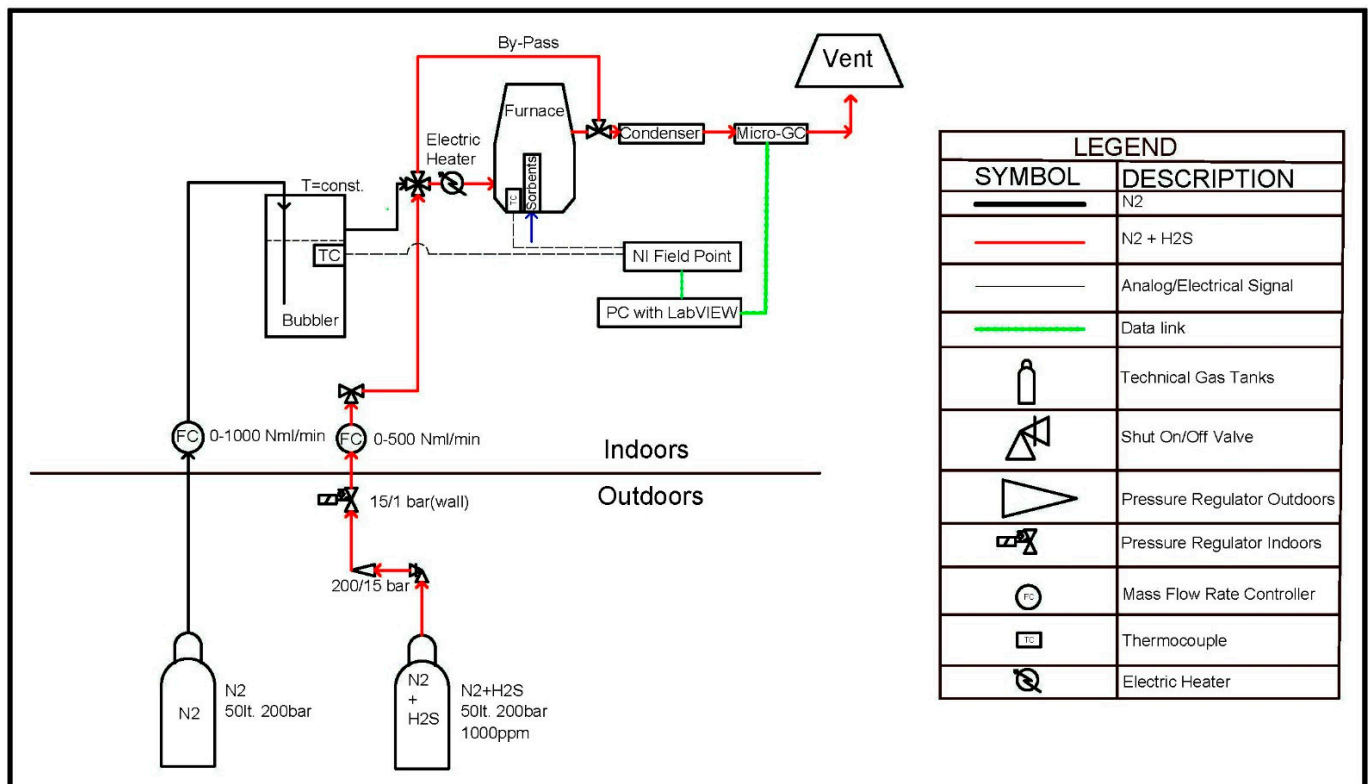

Figure 1. Current experimental setup for Sorbent Testing.

A programmable muffle furnace, Carbolite Gero (30–3000 °C) CWF 11/13 + 3216, was used to obtain a temperature-controlled operation for the sorbent testing. The furnace temperature was controlled via a PID controller acting on a closed-loop control on the temperature reading from the thermocouple integrated into the furnace. An additional thermocouple (type K) was installed at the furnace inlet to observe the temperature of the sorbents. The technical gas distribution system consists of two different technical gases: pure N_2, and the mixture of N_2 and 1000 ppm H_2S to proceed with the experiments inside the reactor.

The gas pressure is established in two different manners: (i) at the first stage (outdoor) from 200 bar to 5–15 bar, and (ii) at the second stage (indoor) from 5–15 bar to the operating pressure of the test bench (around 1.5 bar). As Mass Flow Controllers (MFC), the Bronkhorst EL-Flow is used. The MFC's are connected and controlled via the data

acquisition module/data logger with the proprietary communication protocol Flow-bus of the MFC's. A gas bubbler is kept at constant temperature by a hot-plate magnetic stirrer (Heidolph MR Hei-Tec). It is integrated into the system to humidify the pure N_2 flow as a function of the temperature at the bubbler. Temperature-controlled line heaters are used throughout the pipeline length (hotline) until the entrance of the furnace to prevent condensation after humidifying the flow. The data acquisition and control system consists of National Instruments' cFP-1808 module, which has different modules for analog input, analog output, and thermocouple measurements. The connection is through LAN with RJ45-RJ45 cable. A custom LabVIEW software developed as a web server is used. At the outlet, the gas composition is evaluated by analyzing the results obtained by the Micro-GC, Agilent 990 gas chromatographer, (with an accuracy of $\pm 1\%$ of scale) with its proprietary software Agilent Open Lab Chromatography Data System.

The technical gases, supplied by SIAD, have the following gas purities:

- N_2, 99.999% (impurities H_2O < 5 ppm; O_2 < 5 ppm; C_nH_m < 0.5 ppm; H_2 < 0.5 ppm)
- N_2 99.9999% + H_2S 1000 ppm (with ± 2.1 ppm uncertainty)

While setting up the experimental tests, all sensors and actuators have been calibrated manually. Before each testing period, $N_2 + H_2S$ at 1000 ppm has been sent to the Micro-GC for measurement verification. The system was tested at each junction point before the beginning of each experiment with a special commercial liquid to confirm that there are no leakages. Prior to starting experiments, the pipeline's tubes were saturated with H_2S since tubes can also adsorb H_2S. The operating time depends on the testing conditions (flow, composition, and temperature). The testing procedure after closing the system is as follows: the N_2 gas, that flows through the by-pass of the furnace, is switched to the reactor where steel tubes are heated. Steam is added to the gas stream by the bubbler brought at the right temperature assuring the correct partial pressure value and the consequent volume percentage content. The pipeline after the addition of steam is pre-heated to 150 °C to avoid steam condensation that is added/injected into the system. The tests were conducted without interruption. In case of an interruption, the system is immediately flushed with N_2 gas until experimental parameters return to the original values. After each test, when the system was in the cooling down phase, to preserve the sorbent's properties, the system was flushed again with N_2. Finally, the Micro-GC calibration has been performed after each run. The sorbent is carefully taken out and inspected by weighing and visual inspection. Morphological and structural characterization were performed by using a high-resolution electronic scanning microscope Auriga-Zeiss (SEM), and the PHILIPS PW 1830 diffractometer, respectively. The diffractometer operated using a CuKα source (λ = 1.5418 Å) and a 2θ angle ranging from 25° to 70° at a scan rate of 2θ min^{-1}. Finally, Balmer Emmett and Teller (BET) analysis has been carried out using the Fisons System instrument (model: SORPTY 1750).

3. Results and Discussion

3.1. Adsorption Tests

The conditions for the testing campaign are presented in Table 1, and the parameterization is done between 400 and 600 °C. This temperature range has been selected for the desulfurization temperature near the biomass gasification and SOFC temperatures system. Most of the research has been carried out up until 400 °C. If the temperature of the conditioning could be increased, the energy required to cool down the gas after gasification and heating up would be decreased. The step size is selected as ΔT = 50 °C to find out the 50 °C temperature window, where the sorbent works more efficiently. The experiments are performed for more than 4 h to have enough data to estimate the deactivation model.

Table 1. Sorbent experimental set-up.

| Experimental Conditions	
Sorbent (grams)	0.5 ± 0.001
T (°C)	400–600
N_2 (vol.%)	82
H_2S (ppmv)	410
H_2O (vol.%)	18
P (bar)	0.95–1.05
GHSV (h^{-1})	25,000
N_2 (NmL min^{-1})	250
Total flow (Nml min^{-1})	305 ± 1
Bed Length (BL) (cm)	1.5
Particle diameter(cm)	1.5–3.0

To represent an average content of a biomass gasification syngas, the H_2S and H_2O content have been selected to 410 ppm and 18% in volume, respectively [10].

Moreover, two different tests have been performed varying gas flow rate and bed length (BL) to obtain other values of GHSV equal to 40,000 h^{-1} and 50,000 h^{-1}, respectively. In particular, the flow rate has been increased by 60%, and the BL has been diminished by half, working at 550 °C and 600 °C, respectively.

The exothermic [5] reaction, taking place into the bed, is the following:

$$ZnO_{(s)} + H_2S_{(g)} \leftrightarrow ZnS_{(s)} + H_2O_{(g)}$$
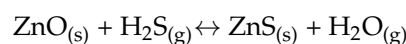
The results of the experimental campaign are plotted in Figures 2–4. Figure 2 shows the effluent H_2S concentration as a function of time with same length bed (BL) and flow rate equal to 1.5 cm and 305 Nml min^{-1}, respectively. Figure 3A shows the linear trend of $\ln(\ln(C_0/C))$ vs. time as the activation model predicts, while in Figure 3B the fitting of breakthrough curves has been reported. The fitting has been obtained by using the kinetic parameters, reported in Table 2, figured out by the analysis of experimental data.
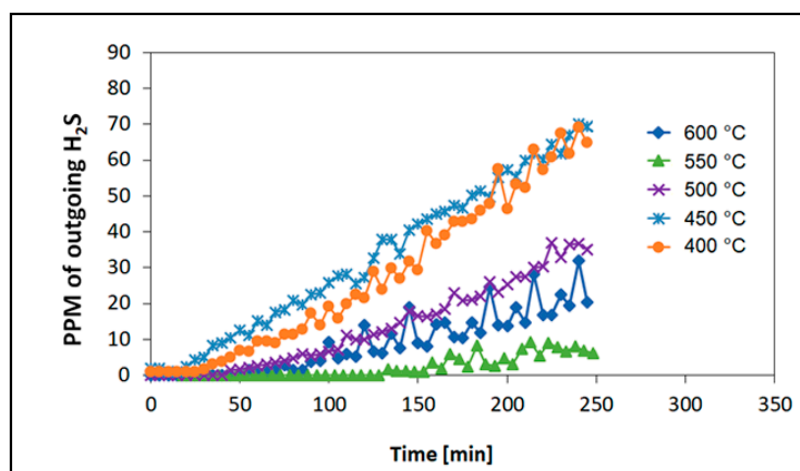
Figure 2. Outlet H_2S concentration vs. time at different temperatures (400, 450, 500, 550, and 600 °C).
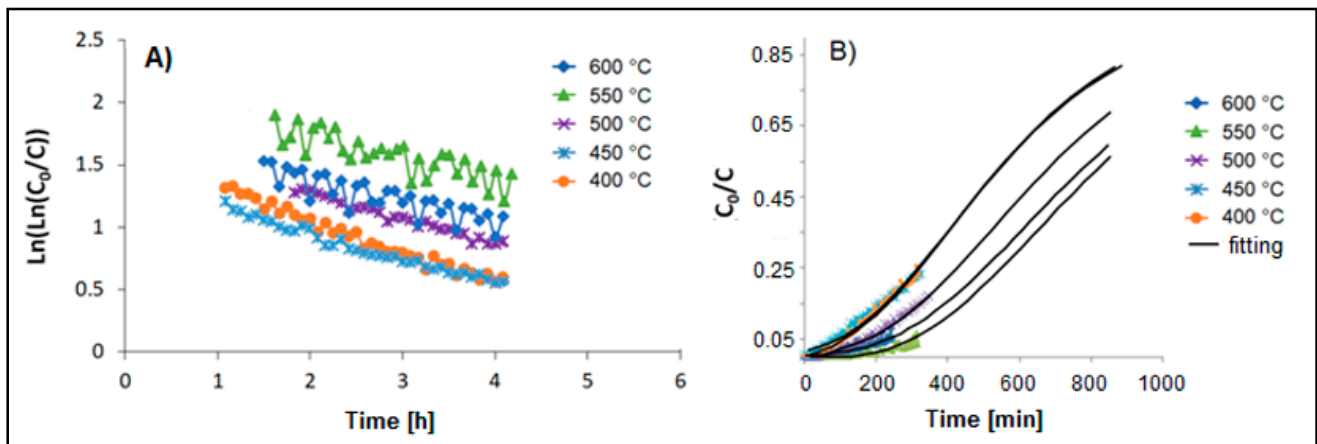
Figure 3. (**A**) Linear trend of $\ln(\ln(C_0/C))$ vs. Time for a temperature ranging from 400 °C to 600 °C; (**B**) Breakthrough curves fitting results with a bed length equal to 1.5 cm and GHSV equal to 25,000 h^{-1}.
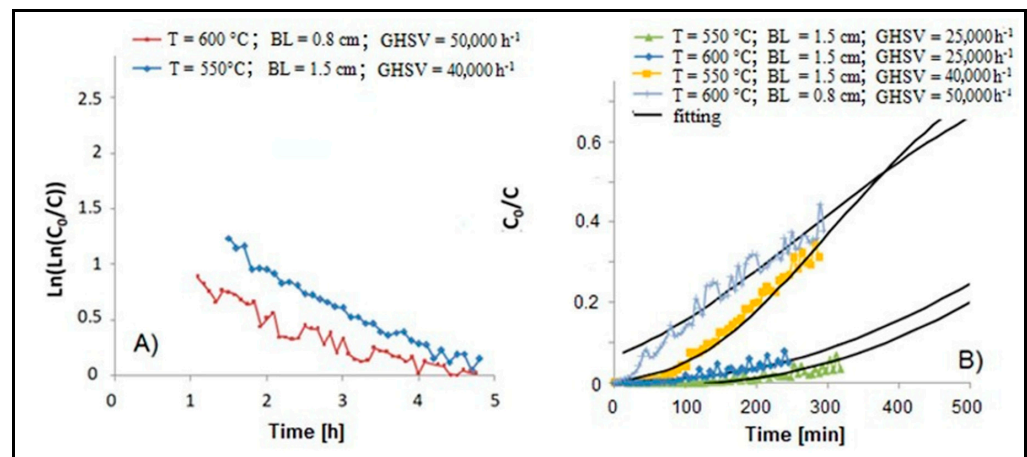

Figure 4. (**A**) Linear trend of $\ln(\ln(C_0/C))$ vs. Time; (**B**) Breakthrough curves fitting results with different GHSV at 550–600 °C and different bed lengths at 600 °C.

Table 2. Linearized deactivation model and breakthrough curves parameters. Obtained by experimental and fitting results.

T [°C]	Bed Length [cm]	GHSV [h^{-1}]	$\ln(\frac{k_0 m_{ads}}{\dot{v}_g})$	k_0 [L g^{-1}h^{-1}]	k_d [h^{-1}]	R^2	t_b [h]	t_s [h]	v_s [cm h^{-1}]	LUB [cm]	MTZ [cm]	SC_b	SC_e
600	0.8	50000	0.99	318	0.226	0.90	0.03	7.5	0.106	0.8	1.60	0.75	27
550	1.5	40000	1.62	895	0.327	0.97	0.70	8.7	0.172	1.38	2.76	5.3	27
600	1.5	25000	1.72	675	0.171	0.71	1.42	14.3	0.104	1.35	2.70	2.9	27
550	1.5	25000	1.90	739	0.182	0.70	2.72	13.6	0.109	1.21	2.42	5.4	28
500	1.5	25000	1.62	525	0.185	0.98	0.92	13.0	0.115	1.39	2.79	1.8	24
450	1.5	25000	1.40	394	0.206	0.97	0.42	11.3	0.132	1.46	2.91	1.0	20
400	1.5	25000	1.45	385	0.212	0.97	0.45	10.8	0.140	1.43	2.86	1.0	19

Instead, Figure 4A depicts the linear trend of $\ln(\ln(C_0/C))$ vs. time for two different cases: when only the BL has been varied, halving its value at 600 °C; while in the other case, when only the total gas flow rate has been increased to 490 Nml min^{-1}, at 550 °C. Moreover, Figure 4B reports a fitting and a comparison with previous conditions. The adsorbed H_2S is calculated at the breakthrough time. In this work, breakthrough time (t_b) was defined as the time from the beginning of sorption to the instant that outlet H_2S concentration reached 2 ppm and the deactivation model has been used. Many models have been used in the literature [28,29], but the deactivation model worked very well in most cases [2,4,30], also for desulfurization adsorption with ZnO [2,4,5,7,31]. For example, Frilund et al. [5] studied the desulfurization of biomass syngas using ZnO-based adsorbents

and analyzed their results utilizing the deactivation model. They obtained a long-term breakthrough curve with a GHSV of 21,000 h^{-1} and an initial H_2S concentration of about 100 ppm. Similarly, H.F. Garces et al. [31] successfully used the deactivation model for their desulfurization adsorption experiment with ZnO sorbent using a GHSV of 47,750 h^{-1} and a temperature ranging from 50 to 400 °C. Therefore, the following deactivation model is taken into account, which neglects external mass-transfer limitations, isothermal conditions, and deactivation of the adsorbent is a first-order equation with respect to the solid surface.

$$-\frac{da}{dt} = k_d C_A^m a^n = k_d a \tag{1}$$

where:

    da/dt is the rate of change of adsorbent activity
    k_d is the deactivation rate constant, h^{-1}
    C_A is the H_2S concentration in the gas phase
    a is the solid active sites.
    As we assume that the deactivation of adsorbent is a first-order equation, n = 1 and m = 0.

$$\ln\left(\ln\left(\frac{C_{A0}}{C_A}\right)\right) = \ln\left(\frac{k_0 m_{ads}}{\dot{V}_g}\right) - k_d t \tag{2}$$

where k_0 is the initial adsorption rate constant, m_{ads} is the adsorbent weight and $\dot{V}_g$ is the total gas flow rate. The evaluation of the deactivation model proposed for the analysis of the experimental data is presented in Figure 3, where Equation (2) is plotted vs. time, obtaining a straight trend with the slope of $-k_d$ and an intercept equaling $\ln\left(\frac{k_0 m_{ads}}{\dot{V}_g}\right)$. Consequently, the adsorption rate constant and deactivation rate constants are calculated. From Figures 3 and 4, it is possible to observe that the experimental data fit quite well.

Therefore, from experimental tests and by using the deactivation model some parameters have been directly calculated as the values of k_0, k_d, sorption capacity at breakthrough (SC$_b$) (g-sulfur/100 g-sorbent), and the breakthrough time t_b. These values are reported in Table 2. In our experiments, k_d decreases when the temperature rises, while the k_0 value increases up to 550 °C then, it diminishes. The trend of k_d values is coherent with that reported by Frilund et al. [5] and Garces et al. [31], but it is not possible to state the same thing for k_0 because for Frilund et al. it decreases with temperature, while the opposite happens for Garces et al. Anyway, the unit of magnitude is quite similar to both cases confirming the accuracy of the results. Concerning the SC$_b$, considering the same H_2S breakthrough concentration (2 ppmv), the values obtained in this work are about one order bigger than those attained by Frilund et al. [5], even if they worked with a lower initial H_2S concentration. In contrast, the SC$_b$ is slightly lower than values reached by Garces et al. [31], but in this case, both the initial and the breakthrough H_2S concentrations are much higher. Furthermore, fitting the breakthrough curves, other parameters such as the equilibrium time (t_e, considered the time needed to reach the same inlet H_2S concentration in the outlet flow), final sorption capacity at equilibrium time (SC$_e$), mass transfer zone length (MTZ, where a concentration profile arises inside the reactor), and stoichiometric time (t_s) have been estimated. The stoichiometric time is defined as the maximum concentration breakthrough time obtainable if the concentration profile into the bed was strictly vertical (plug flow breakthrough); practically, in the presence of the MTZ, the stoichiometric time, t_s, divides it into two equal areas (t_s is equidistant between t_b and t_e). Regarding the parameters above mentioned, the respective results are shown in Table 2. The sorption capacity of the sorbent (SC$_b$) at breakthrough and the breakthrough time (t_b) basically increase with increasing temperature until 550 °C, reaching a value of 5.4 g of sulfur per 100 g of sorbent and 2.72 h, respectively, then they decrease. Indeed, sulfur removal efficiency is kinetically promoted at higher temperatures but, being an exothermic process [5], it is thermodynamically favored at lower temperatures. Moreover, Zn volatilization [21,22] can also cause a decrease in adsorption. This behavior is also

confirmed by the estimated values of SC_e, which are greater at higher temperatures even if the reaction is exothermic, highlighting kinetic limits at lower temperatures. The SC_b determination is relevant for kinetic studies, but the SC_e evaluation is required to know the real quantity of H_2S that can be removed by sorption. Thus, knowing that value, it is possible to determine, for example, the sorbent quantity needed to guarantee the operation of the gas conditioning system for a specific time.

As is reported in the literature $MTZ = 2LUB$ [5] where *LUB* is the length unused bed. These values can be expressed as

$$LUB = L \cdot \left(1 - \frac{t_b}{t_s}\right) \tag{3}$$

Concerning the *LUB* and *MTZ* values, from the breakthrough capacity results, the bed length is not sufficient for the *LUB* sizing concept to be used for the results in this investigation [5]; nevertheless, the concept of the mass-transfer zone can be useful to understand the experimental results, also in this study, and the deactivation model represents the experimental data quite well. In all experiments relative to the mass-transfer zone, the short bed length produces a decrease in the utilization rates and sorption capacity.

Indeed, by halving the bed length, t_b is widely lowered, reaching about 2 min, and SC_e also decreases highly since the bed length is practically equal to the LUB. This means that at breakthrough, most of the bed has remained unused.

However, by increasing the GHSV at 600 °C and 550 °C, there is no change in SC_e. Accordingly, if the bed length does not change, the SC_b does not change either. The saturation velocity (v_s) equal to the ratio between the bed length and the t_s is directly proportional to the supply flow, suggesting that the overall resistance of the process is not a function of GHSV and that the external mass transfer resistance may be neglected as the deactivation model assumes. Furthermore, the presence of MTZ and the slight influence of temperature [32] on the v_s suggests that the global resistance is a function of the intraparticle mass transfer resistance.

Since commercial-scale adsorption processes, due to pressure drop constraints, typically use particle sizes larger than 1000 μm, as in this work, even if the external mass transfer can be neglected, as the deactivation model suggests, the internal intraparticle diffusional resistances and then the intraparticle mass transfer limitations, with this particle size range, are significant.

Therefore, to decrease the internal mass transfer resistance, it would be necessary to act on the particle size [33]. In general, the particle size can affect the mass transport throughout themselves since changing the path of the gas inside the particles, the mass transfer resistance changes as well. Thus, small particles can offer lower intraparticle resistance, whereas decreasing the particle size can increase pressure drops. Therefore, further investigations should be conducted varying the particle size range to understand if the particle size is a critical factor.

Moreover, following the same procedure carried out in the literature [34,35] by plotting $ln(k_0)$ as a function of the reciprocal term of temperature in Kelvin, the Arrhenius plot has been obtained and reported in Figure 5. The apparent activation energy has been calculated. It is about 17 kJ mol^{-1} and its results tend to be quite in line with the value obtained by Karim et al. [35].
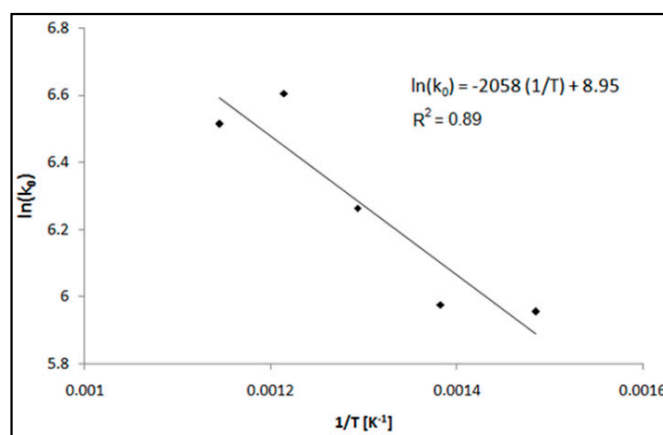
Figure 5. Arrhenius plot for energy activation determination.

3.2. Sorbent Characterization

By analyzing the SEM images, it is possible to clearly observe that the surface of ZnO particles is very porous and made up of very fine grains with heterogeneous morphology and size. Figure 6 shows the morphology of nanoparticles that varies from small spherical particles to big polyhedral nanoparticles and even micro and nanorods. Also, a plate-like morphology is present. The size ranges from microparticles to nanoparticles. By using the BET analysis, the particles specific surface is equal to 43 m^2 g^{-1}.
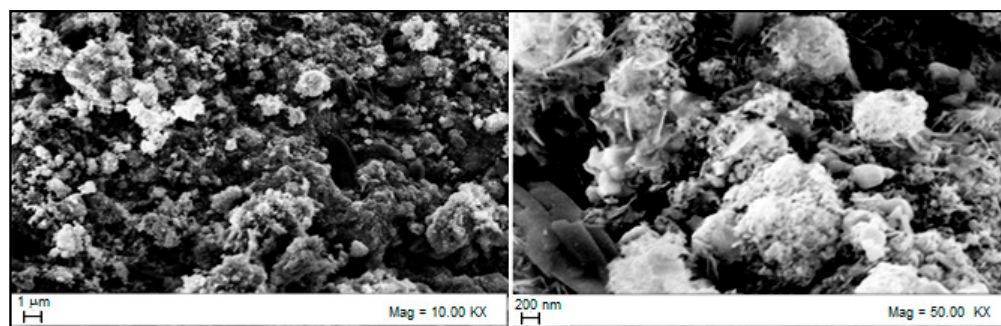
Figure 6. SEM ZnO sorbent before adsorption.

The composition of ZnO particles has been evaluated by EDS analysis and reported in Table 3. In Figure 7, the EDS spectrum and the red/green mapping of the particles, respectively, have been reported, showing mainly the presence of zinc and oxygen, apart from impurities such as aluminum and carbon. The former is present in the pristine material and the latter is due to the sample holder.

Table 3. BET analysis of the pristine sample and after adsorption at breakthrough and equilibrium time at 550 °C.

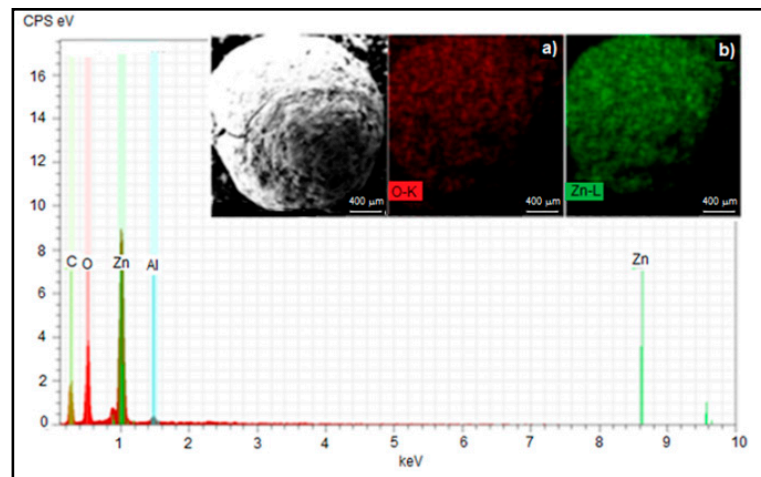| Element	Initial Composition wt%	Composition at Breakthrough Time wt% at 550 °C	Composition at Equilibrium Time wt% at 550 °C
O	20.89	19.14	5.98
S	0	4.53	24.63
Zn	77.72	75.03	68.05
Al	1.39	1.30	1.34

Figure 7. Energy-dispersive X-ray spectroscopy (Elemental Analysis) of sorbent before adsorption. The embedded map includes (**a**) oxygen and (**b**) zinc.

To know the real SC_e, around 0.5 g of sorbent was used to adsorb at 550 °C, for more than a day, until the concentration of the outgoing gas was equal to the incoming one. Then, SEM, EDS, BET, and XRD analyzes were performed on that sorbent.

Figure 8 shows SEM micrographs of particles after the sorption process, the morphology seems to be more homogenous, mainly at higher magnification, likely due to the adsorption process at high temperature. In Figure 9, EDS spectra and the mapping (aided by colors) of the outer surface of ZnO particles after the sorption process have been reported. Elements like Zn, O, and S have been detected along with Al and C due to impurities already described. In this case, the presence of S is abundant, and it seems to be complementary to oxygen, as expected. Furthermore, BET analysis indicates a decrease of particles specific surface that becomes equal to 31 m^2 g^{-1} due to a probable loss of porosity after H_2S adsorption due to a larger volume occupied by ZnS [5]. Finally, SEM and EDS analyses of the internal part of particles are shown in Figures 10 and 11, respectively. From SEM micrographs, also, in this case, the inner morphology appears to be a little bit more homogeneous even if with nanoparticles more agglomerated and sintered, while the previous findings were different compared to the pristine material in terms of composition, as shown in EDS analysis reported in Table 3. In Figure 11, the inner part of ZnO particles is shown along with the colored mapping to depict the location of the three elements. Also, a significant presence of sulfur is detected, while the oxygen presence appears only where sulfur concentration is lower, namely in the middle of the particle.
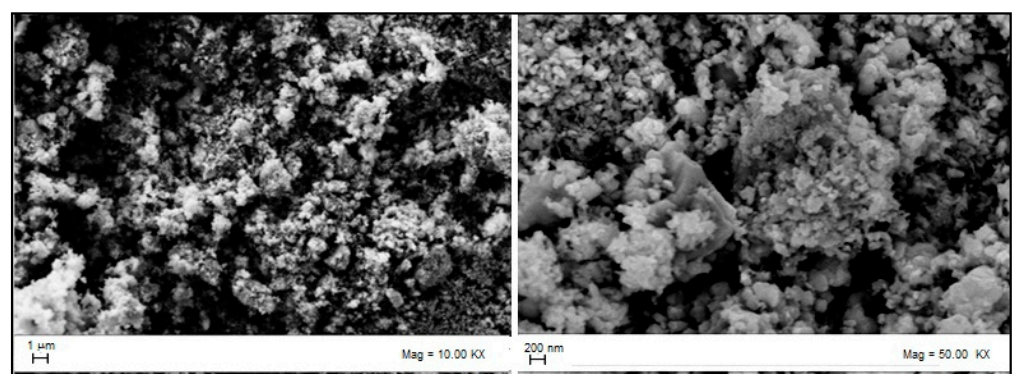

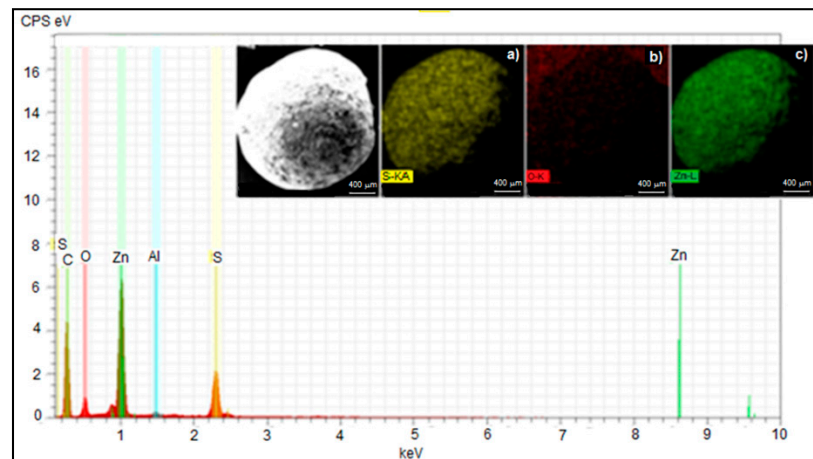**Figure 8.** SEM ZnO sorbent external surface after adsorption.

Figure 9. Energy-dispersive X-ray spectroscopy (Elemental Analysis) after adsorption. The embedded map of elements (**a**) sulfur; (**b**) oxygen; (**c**) zinc also can be seen.
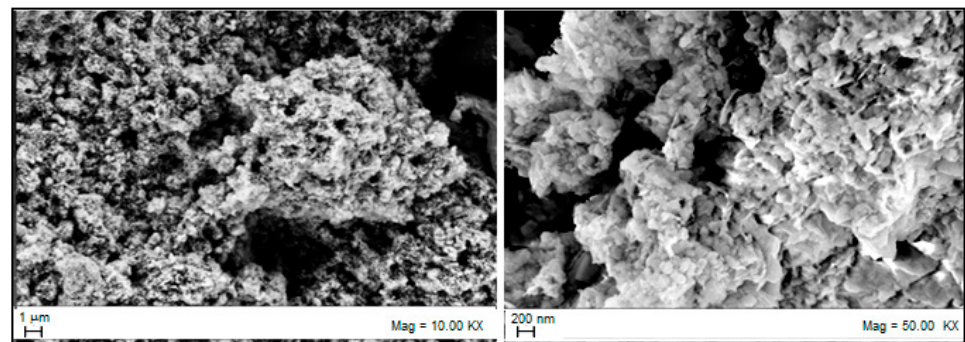

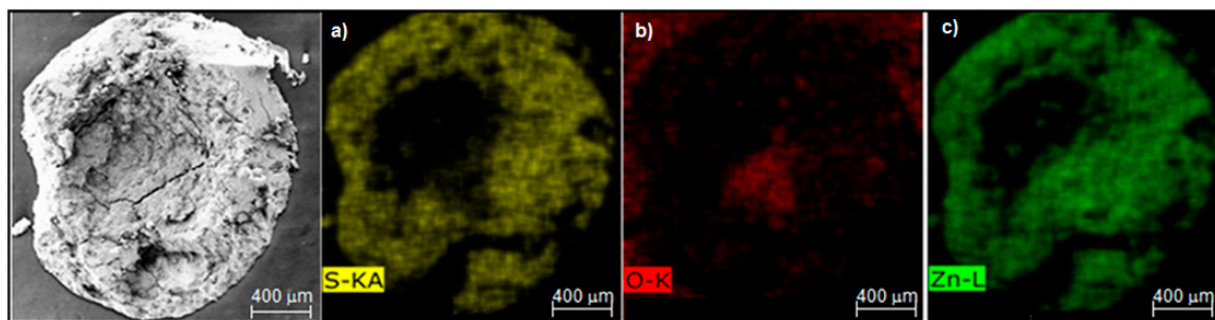**Figure 10.** SEM ZnO sorbent inner part after being used.

Figure 11. Inner part of $ZnO_{(s)}$ particles after being utilized XRD analysis: (**a**) sulfur; (**b**) oxygen; (**c**) zinc.

The data are shown in Table 3. They confirm the results obtained from the breakthrough curves. Hence, this sorbent has a high sulfur adsorption capacity reaching saturation with an amount of adsorbed sulfur equal to about 25 wt% when the temperature is 550 °C.

Moreover, XRD diffractograms confirm the adsorbing capacity. Figure 12a shows the peaks of the pristine material before adsorption and practically only ZnO is present. It exhibits a hexagonal crystalline structure corresponding to the zinc oxide pattern from the crystallography open database (C.O.D. 9004181). The peak profile indicates a material characterized by a scarce crystallinity, as shown by the broadened peaks that typically characterize amorphous materials. After adsorption in Figure 12b, a new phase is present corresponding to the ZnS formation (C.O.D. 9013162) that exhibits a quite amorphous

hexagonal crystalline structure. However, some zinc oxide is still present. For both phases, Miller's indexes are reported.
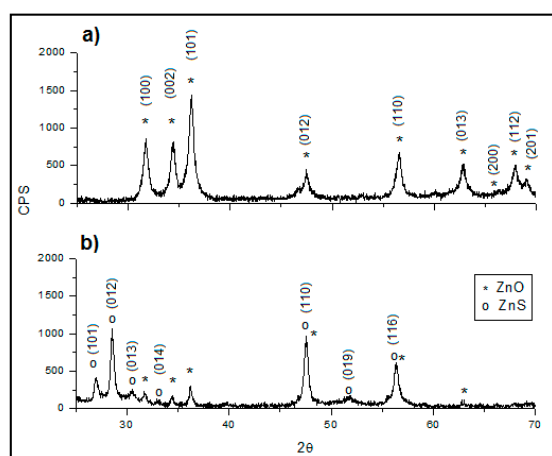

Figure 12. XRD diffractograms of sorbent (**a**) before adsorption, (**b**) after adsorption.

4. Conclusions

The focus of the work is to assess the possibility to approach the gas conditioning upstream condition with the subsequent working temperature of SOFC in a more efficient energy system. Therefore, commercially available zinc oxide has been studied and characterized as a desulfurizing agent in a fixed-bed reactor at high temperatures up to 600 °C. The sorbent's sorption capacity has been measured at different temperatures, as well as the breakthrough curves. The best performances have been obtained at 550 °C, obtaining a sorption capacity of 5.4 g per 100 g of sorbent and a breakthrough time of 2.7 h. Furthermore, the kinetic parameters such as the initial sorption rate constant k_0 and deactivation rate constant k_d have been evaluated in all tested working temperature conditions using the linearized deactivation model. The activation energy has been then calculated to be about 17 kJ mol^{-1}. Moreover, by calculating MTZ and LUB parameters, it has been possible to establish that both the internal intraparticle diffusional resistances and intraparticle mass transfer limitations are significant for these sorbent particles. Furthermore, the sorbent material was characterized by XRD, SEM, BET and EDX analyses before and after adsorption, obtaining coherent results.

Author Contributions: Conceptualization, E.B., A.D.C. and L.D.Z.; Methodology, E.B., A.D.C. and L.D.Z.; Investigation, A.H., A.D. and E.C.; Data Curation, A.H., A.D. and E.C.; Writing—Original Draft Preparation, A.H., A.D., and E.C.; Writing—Review & Editing, A.H., A.D., E.B.; Supervision, E.B. All authors have read and agreed to the published version of the manuscript.

Institutional Review Board Statement: Not applicable.

Informed Consent Statement: Not applicable.

Data Availability Statement: Not applicable.

Conflicts of Interest: The authors declare no conflict of interest.

References

1. Bin Chung, J.; Chung, J.S. Desulfurization of H2S using cobalt-containing sorbents at low temperatures. *Chem. Eng. Sci.* **2005**, *60*, 1515–1523. [CrossRef]
2. Ko, T.-H.; Chu, H.; Liou, Y.-J. A study of Zn–Mn based sorbent for the high-temperature removal of H2S from coal-derived gas. *J. Hazard. Mater.* **2007**, *147*, 334–341. [CrossRef] [PubMed]
3. Ko, T.; Chu, H.; Chaung, L.; Tseng, T. High temperature removal of hydrogen sulfide using an N-150 sorbent. *J. Hazard. Mater.* **2004**, *114*, 145–152. [CrossRef] [PubMed]
4. Yasyerli, S.; Dogu, G.; Ar, I.; Dogu, T. Activities of Copper Oxide and Cu−V and Cu−Mo Mixed Oxides for H2S Removal in the Presence and Absence of Hydrogen and Predictions of a Deactivation Model. *Ind. Eng. Chem. Res.* **2001**, *40*, 5206–5214. [CrossRef]
5. Frilund, C.; Simell, P.; Kaisalo, N.; Kurkela, E.; Koskinen-Soivi, M.-L. Desulfurization of Biomass Syngas Using ZnO-Based Adsorbents: Long-Term Hydrogen Sulfide Breakthrough Experiments. *Energy Fuels* **2020**, *34*, 3316–3325. [CrossRef]
6. Kołodziejczak-Radzimska, A.; Jesionowski, T. Zinc Oxide—From Synthesis to Application: A Review. *Materials* **2014**, *7*, 2833–2881. [CrossRef]
7. Li, L.; Sun, T.; Shu, C.; Zhang, H. Low temperature H2S removal with 3-D structural mesoporous molecular sieves supported ZnO from gas stream. *J. Hazard. Mater.* **2016**, *311*, 142–150. [CrossRef]
8. Wang, X.; Sun, T.; Yang, J.; Zhao, L.; Jia, J. Low-temperature H2S removal from gas streams with SBA-15 supported ZnO nanoparticles. *Chem. Eng. J.* **2008**, *142*, 48–55. [CrossRef]
9. Kim, K.; Park, N. Removal of hydrogen sulfide from a steam-hydrogasifier product gas by zinc oxide sorbent: Effect of non-steam gas components. *J. Ind. Eng. Chem.* **2010**, *16*, 967–972. [CrossRef]
10. Rosso, I.; Galletti, C.; Bizzi, M.; Saracco, G.; Specchia, V. Zinc Oxide Sorbents for the Removal of Hydrogen Sulfide from Syngas. *Ind. Eng. Chem. Res.* **2003**, *42*, 1688–1697. [CrossRef]
11. Jung, S.Y.; Lee, S.J.; Park, J.J.; Jun, H.K.; Lee, T.J.; Ryu, C.K.; Kim, J.C. The simultaneous removal of hydrogen sulfide and ammonia over zinc-based dry sorbent supported on alumina. *Sep. Purif. Technol.* **2008**, *63*, 297–302. [CrossRef]
12. Breck, D.W. *Zeolite Molecular Sieves: Structure, Chemistry and Use*; Breck, D.W., Ed.; John Wiley: New York, NY, USA, 1974; ISBN 978-0471099857.
13. de Oliveira, L.H.; Meneguin, J.G.; Pereira, M.V.; da Silva, E.A.; Grava, W.M.; Nascimento, J.F.D.; Arroyo, P.A. H$_2$S adsorption on NaY zeolite. *Microporous Mesoporous Mater.* **2019**, *284*, 247–257. [CrossRef]
14. Sigot, L.; Ducom, G.; Germain, P. Adsorption of hydrogen sulfide (H2S) on zeolite (Z): Retention mechanism. *Chem. Eng. J.* **2016**, *287*, 47–53. [CrossRef]
15. Ozekmekci, M.; Salkic, G.; Fellah, M.F. Use of zeolites for the removal of H 2 S: A mini-review. *Fuel Process. Technol.* **2015**, *139*, 49–60. [CrossRef]
16. Shen, F.; Liu, J.; Zhang, Z.; Dong, Y.; Gu, C. Density functional study of hydrogen sulfide adsorption mechanism on activated carbon. *Fuel Process. Technol.* **2018**, *171*, 258–264. [CrossRef]
17. Mohammadi, N.; Khani, H.; Gupta, V.K.; Amereh, E.; Agarwal, S. Adsorption process of methyl orange dye onto mesoporous carbon material–kinetic and thermodynamic studies. *J. Colloid Interface Sci.* **2011**, *362*, 457–462. [CrossRef] [PubMed]
18. Nguyen-Thanh, D.; Bandosz, T.J. Activated carbons with metal containing bentonite binders as adsorbents of hydrogen sulfide. *Carbon N. Y.* **2005**, *43*, 359–367. [CrossRef]
19. Nguyen-Thanh, D.; Bandosz, T.J. Effect of Transition-Metal Cations on the Adsorption of H2S in Modified Pillared Clays. *J. Phys. Chem. B* **2003**, *107*, 5812–5817. [CrossRef]
20. Louhichi, S.; Ghorbel, A.; Chekir, H.; Trabelsi, N.; Khemakhem, S. Properties of modified crude clay by iron and copper nanoparticles as potential hydrogen sulfide adsorption. *Appl. Clay Sci.* **2016**, *127-128*, 123–128. [CrossRef]
21. Ko, T.-H.; Chu, H.; Chaung, L.-K. The sorption of hydrogen sulfide from hot syngas by metal oxides over supports. *Chemosphere* **2005**, *58*, 467–474. [CrossRef]
22. Westmoreland, P.; Harrison, D.P. Evaluation of candidate solids for high-temperature desulfurization of low-Btu gases. *Environ. Sci. Technol.* **1976**, *10*, 659–661. [CrossRef]
23. Norheim, A.; Wærnhus, I.; Broström, M.; Hustad, J.E.; Vik, A. Experimental Studies on the Influence of H2S on Solid Oxide Fuel Cell Performance at 800 °C. *Energy Fuels* **2007**, *21*, 1098–1101. [CrossRef]
24. Li, T.S.; Wang, W.G.; Chen, T.; Miao, H.; Xu, C. Hydrogen sulfide poisoning in solid oxide fuel cells under accelerated testing conditions. *J. Power Sources* **2010**, *195*, 7025–7032. [CrossRef]
25. Chen, H.; Wang, F.; Wang, W.; Chen, D.; Li, S.-D.; Shao, Z. H$_2$S poisoning effect and ways to improve sulfur tolerance of nickel cermet anodes operating on carbonaceous fuels. *Appl. Energy* **2016**, *179*, 765–777. [CrossRef]
26. Błesznowski, M.; Jewulski, J.; Zieleniak, A. Determination of H2S and HCl concentration limits in the fuel for anode supported SOFC operation. *Open Chem.* **2013**, *11*, 960–967. [CrossRef]
27. Boldrin, P.; Ruiz-Trejo, E.; Mermelstein, J.; Menéndez, J.M.B.; Reina, T.R.; Brandon, N.P. Strategies for Carbon and Sulfur Tolerant Solid Oxide Fuel Cell Materials, Incorporating Lessons from Heterogeneous Catalysis. *Chem. Rev.* **2016**, *116*, 13633–13684. [CrossRef]
28. Sun, J.; Modi, S.; Liu, K.; Lesieur, R.; Buglass, J. Kinetics of Zinc Oxide Sulfidation for Packed-Bed Desulfurizer Modeling. *Energy Fuels* **2007**, *21*, 1863–1871. [CrossRef]

29. Turton, R.; Berry, D.A.; Gardner, T.H.; Miltz, A. Evaluation of Zinc Oxide Sorbents in a Pilot-Scale Transport Reactor: Sulfidation Kinetics and Reactor Modeling. *Ind. Eng. Chem. Res.* **2004**, *43*, 1235–1243. [CrossRef]

30. Suyadal, Y.; Erol, M.; Oğuz, H. Deactivation Model for the Adsorption of Trichloroethylene Vapor on an Activated Carbon Bed. *Ind. Eng. Chem. Res.* **2000**, *39*, 724–730. [CrossRef]

31. Garces, H.F.; Galindo, H.M.; Garces, L.J.; Hunt, J.; Morey, A.; Suib, S.L. Low temperature H2S dry-desulfurization with zinc oxide. *Microporous Mesoporous Mater.* **2010**, *127*, 190–197. [CrossRef]

32. Joshi, S.Y.; Ren, Y.; Harold, M.P.; Balakotaiah, V. Determination of kinetics and controlling regimes for H2 oxidation on Pt/Al$_2$O$_3$ monolithic catalyst using high space velocity experiments. *Appl. Catal. B Environ.* **2011**, *102*, 484–495. [CrossRef]

33. Eshraghi, A.; Mirzaei, A.A.; Rahimi, R.; Atashi, H. Fischer-Tropsch Synthesis on Fe-Co-Pt/γ-Al$_2$O$_3$ catalyst: A mass transfer, kinetic and mechanistic study. *Korean J. Chem. Eng.* **2020**, *37*, 1699–1708. [CrossRef]

34. Ko, T. Fitting of Breakthrough Curve by Deactivation Kinetic Model for Adsorption of H2S from Syngas with Zn-Contaminated Soil. *Asian J. Chem.* **2015**, *27*, 865–869. [CrossRef]

35. Hassan, K.H.; Khammas, A.-A.; Rahman, A.M. Zinc Oxide Hydrogen Sulfide Removal Catalyst/ Preparation, Activity Test and Kinetic Study. *Al-Khwarizmi Eng. J.* **2008**, *4*, 74–84.